Journal of
Applied Crystallography
ISSN 0021-8898
Editor: **Anke R. Pyzalla**

High hydrostatic pressure small-angle X-ray scattering cell for protein solution studies featuring diamond windows and disposable sample cells

Nozomi Ando, Pascale Chenevier, Martin Novak, Mark W. Tate and Sol M. Gruner

J. Appl. Cryst. (2008). **41**, 167–175

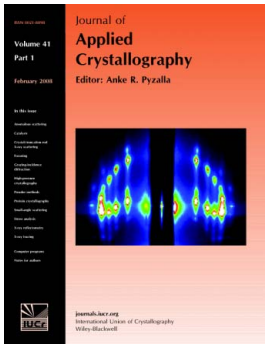

Journal of
Applied Crystallography
ISSN 0021-8898

Received 28 September 2007
Accepted 7 November 2007

High hydrostatic pressure small-angle X-ray scattering cell for protein solution studies featuring diamond windows and disposable sample cells

Nozomi Ando,[a] Pascale Chenevier,[a]‡ Martin Novak,[a] Mark W. Tate[a] and Sol M. Gruner[a,b]*

[a]Department of Physics, Cornell University, Ithaca, NY 14853, USA, and [b]Cornell High Energy Synchrotron Source, Cornell University, Ithaca, NY 14853, USA. Correspondence e-mail: smg26@cornell.edu

A high-pressure cell for synchrotron small-angle X-ray scattering (SAXS) studies of protein solutions is described. The design was optimized for use at up to 400 MPa in liquid pressure and with 8–12 keV X-rays with particular emphasis on the ease of use. The high-pressure cell was fabricated from corrosion-resistant Inconel 725 (Special Metals Corporation, Huntington, WV, USA) and featured Poulter-type windows [Poulter (1932). *Phys. Rev.* **40**, 861–871]. Flat natural diamonds, 500 µm thick, were recycled from diamond anvil cells and were shown to perform well as high-pressure SAXS windows. For a simple and effective method of sample isolation, disposable plastic sample cells with a defined path length and reproducible parasitic scattering were designed. These sample cells enable efficient use of synchrotron time. The cells facilitate rapid and easy sample changes, eliminate the need to clean the cell between sample changes, and reduce the sample volume to as low as 12 µl. The disposable cells can also be used separately from the high-pressure cell for SAXS measurements at ambient pressure and temporary storage of samples. The performance of the apparatus is demonstrated with T4 lysozyme.

1. Introduction

Hydrostatic pressure in the range of several hundred megapascals has been shown to stabilize a variety of protein states (Bridgman, 1914; Heremans & Smeller, 1998; Silva & Weber, 1993; Gross & Jaenicke, 1994). Like temperature, pressure can shift the equilibrium between folded and unfolded configurations or the association equilibrium of multimeric aggregates and subunit domains. Subunit dissociation of low molecular mass multimers (Paladini & Weber, 1981; Pin *et al.*, 1990) and unfolding of monomeric globular proteins (Zipp & Kauzmann, 1973; Panick *et al.*, 1998, 1999; Paliwal *et al.*, 2004; Meersman *et al.*, 2002) have both been observed to occur at several hundred megapascals for proteins under otherwise native conditions. The effects of pressure on kinetics, enzymatic activity, misfolding, amyloid fibrils and large macromolecular assemblages such as viral capsids have also been documented (Brun *et al.*, 2006; Northrop, 2002; Ferrão-Gonzales *et al.*, 2000; Torrent *et al.*, 2005; Silva *et al.*, 1996). Experimental and theoretical efforts to understand the mechanism of these pressure effects are ongoing (Frye & Royer, 1998; Hummer *et al.*, 1998; Royer, 2002; Paliwal *et al.*, 2004; Collins *et al.*, 2005; Harano & Kinoshita, 2006; Imai *et al.*, 2007).

Various techniques have been adapted to study the pressure effects on proteins (Paladini & Weber, 1981; Ruan & Balny, 2002; Akasaka & Yamada, 2001; Jonas, 2002; Winter, 2002; Fujisawa *et al.*, 1999; Dzwolak *et al.*, 2002; Mozhaev *et al.*, 1996). Scattering techniques such as small-angle X-ray (SAXS) and neutron scattering (SANS) are useful for probing global structural changes that accompany pressure-induced unfolding or subunit dissociation. These techniques are especially useful in conjunction with other methods adapted for high-pressure studies, such as fluorescence and absorption spectroscopy, Fourier transform infrared (FT–IR) spectroscopy, NMR, and X-ray crystallography. Unfortunately, there is no commercially available SAXS cell that is suitable for high-pressure studies on protein stability at synchrotron sources. Several documented designs exist (Woenckhaus *et al.*, 2000; Pressl *et al.*, 1996; Nishikawa *et al.*, 2001; Erbes *et al.*, 1996), but none meets the specific need for a cell that is easy to use featuring an effective mechanism to isolate very small amounts of protein. This article describes modifications to one of these designs to meet our requirements.

The main design feature of a high-pressure cell is the high-pressure window. For solution SAXS studies of proteins, the windows must operate at biologically relevant pressures of several hundred megapascals while allowing sufficient transmission of the weak scattering signal from proteins in solution. As background subtraction is necessary, it is critical to

‡ Present address: DRECAM/SPEC, CEA/Saclay, 91191 Saclay Cedex, France.

reproduce the sample path length, the parasitic scattering from the windows, and the internal pressure and temperature of the cell. In these regards, high-pressure X-ray diffraction cells such as the diamond anvil cell or the cylindrical beryllium cell are inappropriate for protein solution SAXS. Diamond anvil cells lack fine control of the sample path length and internal pressure in this pressure range. Geometric considerations prevent the simultaneous optimization of the maximum operating pressure and transmission of the beryllium cell.

A window geometry that has been effective for high-pressure SAXS is the Poulter-type window, a high-pressure window initially designed for optical studies (Poulter, 1932; Woenckhaus *et al.*, 2000; Pressl *et al.*, 1996; Nishikawa *et al.*, 2001; Erbes *et al.*, 1996). We paid particular attention to the design of Woenckhaus *et al.* (2000), which featured Poulter-type window assemblies composed of flat diamonds secured against the apertures with window-retaining screw caps, and adapted it to our high-pressure SAXS cell. For the window material, type IIa diamonds with low nitrogen content are preferred, to minimize the parasitic scattering. However, we took the economical approach of recycling retired diamond anvil cells to produce diamond discs, 500 µm thick. We found that even a strongly scattering diamond can perform satisfactorily if it displays reproducibility and has very little stress-induced variability in parasitic scattering.

Another important but often overlooked feature of a high-pressure cell is the method of sample isolation. Generally, pressure is generated by an external fluid or gas pump, necessitating a means for separating the sample from the pressurizing medium. One method is to inject the sample directly into the sample chamber of the high-pressure cell, then close the chamber with a piston that separates the sample and pressurizing medium (Nishikawa *et al.*, 2001). This method has two obvious advantages; additional parasitic scattering from an internal cell is eliminated and the cell windows do not have to be disassembled to load samples. However, this method also presents two major difficulties. As the sample must occupy small spaces in the sample chamber, cleaning becomes difficult. Our experience is that cleaning the cell, which was essential for proper background subtraction, necessitated the complete and tedious disassembly of the high-pressure cell. Minimizing the sample volume to less than 100 µl could not be achieved without the inclusion of a spacer, but the use of a spacer further introduced small spaces that were difficult to clean. The second drawback of this method is that biological buffers, which are often highly saline, alkaline or acidic, are very corrosive to metal chambers at high pressure.

Alternatively, the sample can be encapsulated in an internal cell with a piston or a soft membrane that isolates the sample while transmitting the pressure (Erbes *et al.*, 1996; Pressl *et al.*, 1996). We adopted the encapsulation method by fabricating disposable internal cells from acrylic laminates and Kapton windows. To avoid the problems with background subtraction that arise from using containers without a defined path length, such as glass X-ray capillaries, we designed these sample cells to isolate the sample from the pressurizing medium while maintaining a fixed sample path length between two flat windows. The multi-functional sample cells reduce the sample volume to as low as 12 µl, eliminate the need to clean the high-pressure cell between sample changes, and allow faster sample changing. They can also be used separately from the high-pressure cell for ambient-pressure SAXS experiments and short-term sample storage. The transparent body of the sample cell allows inspection for and removal of air bubbles. Reproducible parasitic scattering from the sample cells enabled the sample and buffer solutions to be contained in separate sample cells. Filled sample cells were loaded through a high-pressure window port without any compromise of the high-pressure cell's robustness or reproducibility.

All components of the high-pressure cell were fabricated from corrosion-resistant Inconel 725 alloy (Special Metals Corporation, Huntington, WV, USA) and specified such that the elastic limit of each component exceeded the highest operating pressure of 400 MPa. The final design permits a maximum resolution of 17.4 Å (q = 0.36 Å^{-1}) with an 8 keV 400 µm square beam and 8.8 Å (q = 0.71 Å^{-1}) with a 12 keV 250 µm square beam where $q = (4\pi/\lambda)\sin(\theta/2)$. The performance of the high-pressure cell and internal sample cells is demonstrated by data taken on a T4 lysozyme mutant.

2. Experimental considerations

2.1. SAXS requirements

Protein solution SAXS requires careful subtraction of the background scattering before data analysis, and therefore two measurements are taken at each sample condition. Achieving a satisfactory background subtraction requires the minimization of parasitic scattering from the system and reproducibility of the conditions. Samples are commonly contained in transmission-style cells with a fixed path length, and the window materials are chosen carefully. Windows benefit from being as thin and uniform as possible to optimize the transmission and reproducibility while minimizing the parasitic scattering. Typical SAXS windows include low-Z materials such as beryllium and diamond, thin polymer films and thin sheets of mica. The scattering signal is optimized when the sample path length is approximately equal to the attenuation length, which for aqueous solutions is 1–3 mm for 8–12 keV X-rays.

In designing the SAXS cell, the length scales of the samples must be considered. The momentum transfer, q, is a function of X-ray wavelength, λ, and the scattering angle, θ. At a fixed X-ray wavelength, the resolution limit or maximum q that can be collected unobstructed from a sample cell is determined by the window thickness, window aperture and irradiated sample volume (Pressl *et al.*, 1996), while the minimum accessible q is often determined by the parasitic scattering of the system. For many SAXS experiments, low-q data are essential for data analysis. Guinier analysis is particularly demanding as the q range over which a Guinier fit is valid moves to lower q with an increase in protein size.

Finally, the materials chosen for the SAXS cell should not interact with the sample. In addition to chemical resistance, the hydrophobicity and charge of the window materials should be considered when dealing with highly charged or aggregating samples. Minimizing the sample volume is also desirable as biological samples are often expensive.

2.2. High-pressure requirements

When selecting materials for high-pressure parts, the yield strength and corrosion resistance should be considered. As the interior of a pressure vessel is typically made by drilling a solid piece of metal, the elastic limit of a cylindrical vessel under pressure can be used as a guide to the yield strengths required. The pressure differential across the wall at which the cylinder will yield, ΔP, can be described as follows (Spain & Paauwe, 1977):

$$\Delta P = (Y/3^{1/2})(1 - \omega^2), \tag{1}$$

where Y is the yield strength of the material, and ω is the ratio of the outer to inner radii of the wall. Corrosion is detrimental to high-pressure seals, which depend upon good contact, and should therefore be considered in the material selection. Stress-corrosion cracking is also a concern at high pressure. Corrosion resistance can also be affected by the presence of other materials; for example, we have observed galvanic corrosion at high pressure when a brass piece was inserted in a stainless-steel high-pressure cell that only contained deionized water.

For high-pressure applications, strong low-Z materials such as beryllium and diamond are used as X-ray windows. Diamond is preferred because of the toxicity of beryllium oxide dust. Diamond is also convenient for its chemical inertness and transparency to a wide spectrum of radiation, enabling visual inspection of samples and the use of non-X-ray probes.

Two types of seals are useful in designing a high-pressure cell. Cone seals are simple and reliable seals that are used for connecting standard pressure tubing. A cone seal connection is therefore convenient for connecting the high-pressure cell to a pressure generator. As these seals function by deformation, they are not recommended for parts that cannot be easily replaced or require precise positioning such as window holders. The Bridgman unsupported area seal can be applied in various forms to create effective high-pressure seals. Most notably, it is utilized in Poulter-type window geometries to seal flat windows against apertures (Poulter, 1932). An anti-extrusion ring can also operate on this principle in order to seal a clearance between mating high-pressure parts (Eremets, 1996).

To create a good Poulter-type window, the window and window holder must make good contact. In our experience, a deformable gasket between the surfaces is unnecessary and, more importantly, is inappropriate for SAXS where the window position must be reproducible. Good contact should be achieved by polishing the hard-metal window holder to a good flatness and mirror finish. The contact at the interface can be evaluated by observing the interference fringes under a microscope. At low pressure, a window retainer is required to assist the seal. Glues are not suitable for this task if temperature variation is desired. For biologically relevant temperatures, a screw cap (Fig. 1) has been found to be adequate (Woenckhaus *et al.*, 2000). The elastic limit of a window in an unsupported area seal can be estimated using the following equation for an unclamped plate against a circular hole (Holzapfel & Isaacs, 1997):

$$P_{\max} = \frac{8}{3}\left(\frac{T}{R}\right)^2 \frac{Y}{3+\sigma}, \tag{2}$$

where the yield pressure, $P_{\max}$, is determined by the window thickness, T, the radius of the unsupported hole, R, the yield strength of the window, Y, and the Poisson ratio of the window, σ. Similarly, the deflection of the window with pressure should be noted.

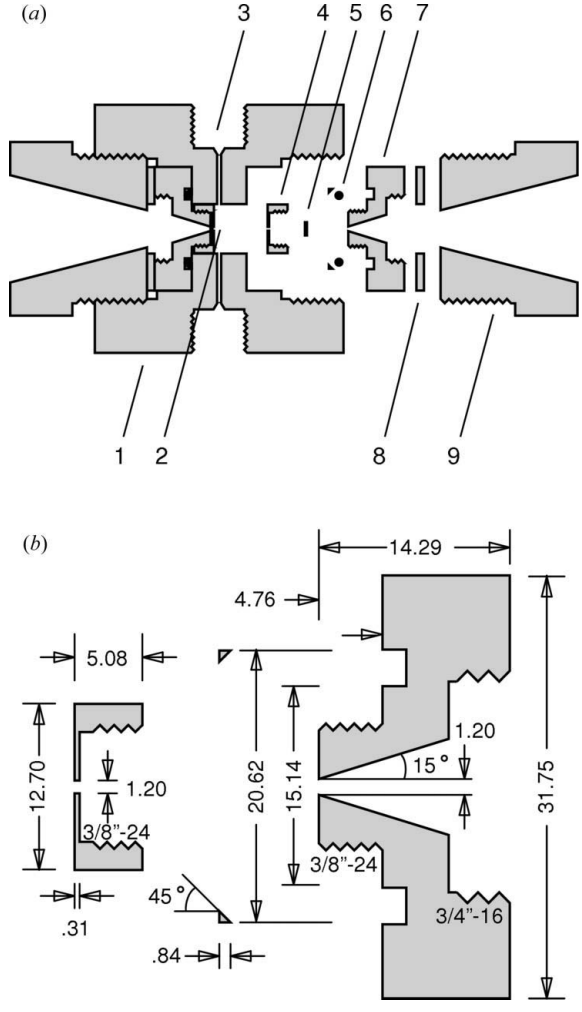

Figure 1
(*a*) Cross-sectional diagram of the high-pressure SAXS cell. 1: 63.50 × 63.50 × 63.50 mm Inconel 725 cell body. 2: Sample cell chamber. 3: Pressure connection. 4: Inconel 725 window retaining screw cap. 5: Diamond window. 6: Viton O-ring and brass anti-extrusion ring. 7: Inconel 725 window holder. 8: Brass jam washer. 9: Stainless-steel closure nut. (*b*) Dimensional drawings of window holder, anti-extrusion ring and window-retaining cap. Units are in millimetres unless otherwise specified.

Table 1
Estimates of material properties used for high-pressure cell design.

Data from Special Metals Corporation, Huntington, WV, and Field (1979).

Inconel 725 age-hardened yield strength	1029 MPa
Diamond yield strength	750 MPa
Diamond Poisson ratio	0.1

3. Description of design

3.1. High-pressure SAXS cell

Using the experimental considerations outlined above, we designed the high-pressure SAXS cell to meet the following criteria. The elastic limit of each design component should exceed 400 MPa with the highest accessible q being approximately 0.4 Å^{-1} for an 8 keV 400 µm square beam and a path length between 1 and 3 mm. Conservative estimates of material properties were used (Table 1). The final specifications and dimensions are summarized in Table 2 and Fig. 1.

The cell body, window holders and window-retaining screw caps were machined from Inconel 725 alloy, chosen for its strength and resistance to corrosion and stress-corrosion cracking. Prior to machining, the stock alloy was annealed by heating at 1283 K for 1 h in a pre-heated furnace, followed by air-cooling. Following machining, the cell components were age-hardened to their final strength by heating for 8 h at 1033 K in a pre-heated furnace, after which the temperature was lowered to 922 K at 311 K per hour. The components were then held at 922 K for 8 h and finally allowed to air-cool. All heat treatments were performed in air with no effort made to provide a protective atmosphere. Natural diamonds recycled from diamond anvil cells were used as windows. Flat diamonds with the faces normal to the [100] axis were prepared by grinding above and below the anvil girdles to a final thickness of 500–560 µm with a parallelism of a few milliradians. Each window holder was fabricated with an aperture of 1.2 mm diameter, with a 30° full-angle conical opening formed by electrical discharge machining. The window mounting face of the window holder was polished using 0.5–1 µm diamond lapping films (PSI-1601D-6, PSI-1601D-6 A, PSI-16.5D-6A; Precision Surfaces International, Houston, TX, USA) wetted with distilled water. Once good contact between the diamond and window holder was established, the diamonds were fixed in place with the window-retaining screw caps.

The assembled window holders are plugged into the window ports of the cell body in a transmission orientation such that the distance between the window caps is approximately 2.3 mm. The distance between the diamond faces is 3.1 mm. The seal between the window holder and cell body is created by an O-ring assisted by a brass anti-extrusion ring (Fig. 1). With the anti-extrusion ring, a Viton O-ring (2–113 75D Viton; MARCO Rubber & Plastic Products Inc., N. Andover, MA, USA) can be used reliably to 400 MPa at room temperature and does not require replacement during the course of a typical synchrotron experiment. The window holders are torqued into the window ports with a stainless-steel closure nut and a brass jam washer in between. The compression of the jam washer corrects for slight differences in the parallelism of the closure nut and window holder. The threads of the closure nuts are protected with a thin layer of molybdenum grease. The required closure torque is 120 N m.

Table 2
Final high-pressure cell specifications.

Window–window distance	3.1 mm
Cap–cap distance	2.3 mm
Sample path length	2 mm
Minimum sample volume	12 µl
Aperture diameter	1.2 mm
Aperture opening angle	30°
Diamond diameter	3.3 mm
Diamond thickness	500–560 µm
Yield pressure of high-pressure cell	400 MPa
Maximum q with 8 keV 400 µm square beam	0.36 Å^{-1}
Maximum q with 12 keV 250 µm square beam	0.71 Å^{-1}

The cell has two 1/4 inch (6.35 mm) cone seal pressure connections with 1 mm diameter channels that lead to the central chamber. One connection is used as the pressure feed, while the other may be used for another purpose, such as a temperature probe. A 1/4 inch male to 1/8 inch (3.18 mm) female adapter (HM4HF2; High Pressure Equipment Co., Erie, PA, USA) is used to protect the pressure feed from frequent connections and releases. The high-pressure cell is connected to an external pump (Cat. No. 37–6.75–60; High Pressure Equipment Co.) with 1/8 inch pressure tubing through a custom-built stainless-steel high-pressure reservoir. Inside the reservoir, a piston separates water, used as the pressurizing medium in the high-pressure cell, from Fluorinert (FC-77; 3M, St Paul, MN, USA), the pressurizing fluid in the pump. The use of Fluorinert is highly desirable as it is noncorrosive. Unfortunately, Fluorinert scatters X-rays strongly, so water is used inside the high-pressure cell. Only a small torque of 8.5 N m is required to fasten the 1/8 inch pressure tubing to the high-pressure cell, allowing the connection to be made on the beamline. To prevent corrosion of the high-pressure cell, it is never left filled with water or under pressure when not in use. The cell is disassembled and dried in a vacuum oven before storage. The pump was fitted with a custom-built motorized control.

3.2. Internal sample cell

Isolation of the sample from the pressurizing medium is accomplished with a disposable plastic sample cell (Fig. 2). The cell serves the multiple purposes of minimizing the sample volume, facilitating sample changes, providing temporary storage and functioning outside the high-pressure cell for ambient-pressure SAXS.

The sample cell is composed of thin polymer film windows glued on the faces of custom-fabricated laser-cut acrylic laminates of 12.65 mm diameter and 2 mm thickness (ALine Inc., Redondo Beach, CA, USA). The laminates are constructed from cast acrylic sheets joined by 0.002 inch-thick pressure-adhesive film (467MP; 3M). Cast acrylic was chosen for its thickness tolerance and bio-compatibility. The laminate

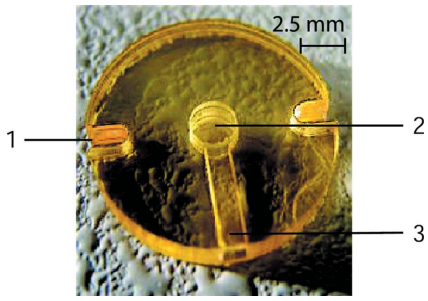

Figure 2
Sample-isolating cell contained within the high-pressure cell made of a cast acrylic body and Kapton windows. 1: Side grooves for removal from high-pressure SAXS cell. 2: Sample chamber. 3: Loading channel and sample reservoir. The sample cell maintains a fixed path length for solution scattering with the pressure transmitted *via* a grease piston in the loading channel. This facilitates rapid sample changing and eliminates the need for cleaning the high-pressure cell.

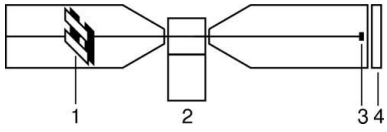

Figure 3
Schematic diagram of the beamline layout for SAXS experiments. 1: Helium-enclosed slits which define beam. 2: Sample assembly on *X*–*Z* translation stage. 3: PIN diode beamstop in vacuum flight path which measures transmitted intensity. 4: CCD X-ray area detector.

body has hole (2.5 mm diameter) through the center and a 1.2 × 1.0 mm channel that spans the edge of the body and the central hole. To complete the construction of a sample cell, 7.5 µm Kapton windows (Spectromembrane No. 3022; Chemplex Industries, Palm City, FL, USA) were stretched flat and glued onto each face. We found that the pressure-adhesive film was not strong enough to maintain the flatness of the films under pressure. Therefore, we applied a thin layer of cyanoacrylate glue (Brush-on Superglue; Loctite, Rocky Hill, CT, USA) on each laminate. After wiping the excess to prevent the glue from wetting the central hole through which the X-rays will pass, the sticky face is placed on a Kapton window that is stretched flat over a support (Cat. No. 1060; Chemplex). An advantage of using cast acrylic cells is that there is sufficient time, *e.g.* up to 30 s, to perform this step successfully. In our experience with acetal homopolymer cells, much less time was available for this step. Once a face is glued, the cell is allowed to cure for several hours, and the process is repeated for the other face. Finally, the excess window material is trimmed from the cell. The completed sample cell has two flat windows, and the path length is determined by the thickness of the laminate body.

Samples are loaded into the central chamber of the sample cell from the side channel using a syringe needle and plugged with vacuum grease (High Vacuum Grease; Dow Corning, Midland, MI, USA). The sliding grease plug acts as a pressure-transmitting piston to prevent the formation of a pressure differential across the windows and thus allows the maintenance of a constant sample path length under pressure. The space in the loading channel also acts as a sample reservoir to account for volume reduction under pressure. A minimum sample volume of approximately 12 µl is required to prevent the grease plug from entering the sample chamber at 400 MPa. The loaded sample cell is placed into the high-pressure cell through a window port. The sample cell fits snugly in the high-pressure cell, assuring alignment of the sample with the diamond windows. Side grooves facilitate removal of the sample cell from of the high-pressure cell with tweezers.

4. Performance and results

4.1. Experimental setup

All of the SAXS measurements were performed at the Cornell High Energy Synchrotron Source (CHESS) G1 Station. To test the performance of the internal sample cells, they were used separately from the high-pressure cell in a conventional ambient-pressure SAXS setup (Fig. 3). Multiple sample cells were mounted side-by-side in a card-shaped brass holder with 1.2 mm apertures. Each sample cell was reused for alternating buffer and protein measurements. Upstream of the sample, a 10 keV 300 × 300 µm beam was defined by helium-enclosed slits. Downstream of the sample, a 1.25 m vacuum flight path (> 30 mTorr) was installed between the sample and a home-built 1024 × 1024 pixel X-ray area CCD detector. A PIN diode beamstop positioned close to the detector blocked the nonscattered beam while recording the transmitted intensity. Beamline components were positioned as closely together as possible to minimize air scattering. The X-ray flux at the sample was approximately 10^{12} photons per second to within a factor of two.

A similar beamline setup with a 12 keV 250 × 250 µm beam was used to test the performance of the high-pressure cell. Protein solution and buffer were filled in separate internal sample cells up to a few hours in advance of each experiment. As the sample cell path length varies slightly from piece to piece, the sample cells were individually measured with a caliper and matched to within 10 µm. After loading a sample cell, the high-pressure cell was fixed tightly in a copper water bath controlled thermostating jacket on an *X*–*Z* translation stage with the windows normal to the beam. The sample was aligned by centering the aperture with an attenuated beam before measurement of a new sample and was periodically checked for drift in beam position. The cell position relative to the beam did not vary more than 30 µm between sample and buffer exposures. This was sufficient to reproduce the parasitic scattering from the cell.

An exposure time of 1 to 10 s was used for each SAXS image to minimize radiation damage. Lead tape was used to cover vertical strip of 20–30 pixel width along one edge of the detector face, allowing measurement of the average zero-offset of every row of pixels. Each SAXS image was treated with a row-by-row zero-offset subtraction, distortion and intensity correction, and shadow masking. Averaging of multiple exposures taken under the same condition was performed in cases where changes such as those caused by

radiation damage were undetected. Diffraction from silver behenate, a SAXS calibrant with a lamellar spacing of 58.376 Å (Huang *et al.*, 1993; Blanton *et al.*, 1995), was used to locate the beam center and convert from image pixel number to q. The corrected detector images were azimuthally integrated about the beam center and normalized by a PIN diode reading to produce a one-dimensional scattering profile, $I(q)$ *versus* q. The corresponding buffer profile was subtracted from that of the protein solution without any scaling. Data treatment and analysis were performed with a suite of custom programs written in C and Matlab (The Mathworks, Natick, MA, USA).

Wild-type (WT) and the L99A mutant of cysteine-free T4 lysozyme (C54T/C97A) were kindly provided by Professor Brian Matthews and coworkers (University of Oregon at Eugene). Samples were dialyzed against 50 m*M* glycine HCl, pH 3.0 buffers at various NaCl concentrations in microdialysis buttons (HR3-362; Hampton Research, Aliso Viejo, CA, USA) closed with a 10 kDa molecular cut-off dialysis membrane (Cat. No. 68100; Snakeskin Tubing, Pierce Biotech, Rockford, IL, USA). The protein solutions were adjusted to various final concentrations of 4–25 mg ml^{-1} by UV absorption measurement. All experiments were performed at room temperature.

4.2. Performance of acrylic sample cells

The performance of the sample cells was first tested separately from the high-pressure cell. SAXS profiles of the same buffer in two separate sample cells with matched path lengths were nearly identical in the q range investigated. Typical results are shown in Fig. 4. The reproducibility of the parasitic scattering from the sample cells supports the use of separate cells for protein solution and its corresponding buffer. Background subtraction was also straightforward and did not require scaling other than transmission normalization. Fig. 5 shows typical data taken from L99A T4 lysozyme in the sample cell separately from the high-pressure cell. A Guinier fit, *e.g.* $I(q) \propto \exp(-R_g^2 q^2/3)$, of this data over q = 0.024–0.076 Å^{-1} gave a radius of gyration, R_g, of 16.5 (3) Å.

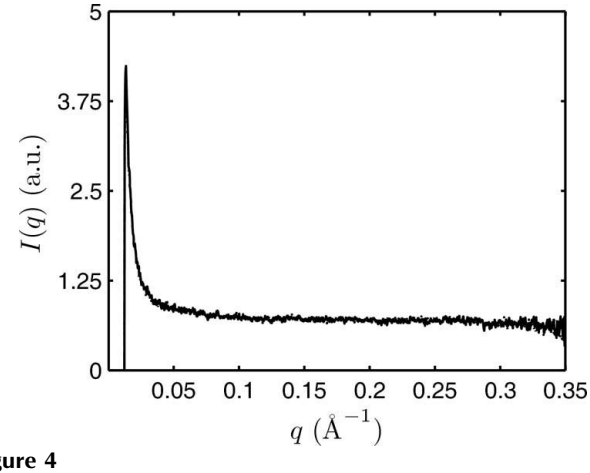

Figure 4
Transmission-normalized scattering profiles of 50 m*M* glycine pH 3.0 buffer. Shown are data taken from two different acrylic sample cells separately from the high-pressure cell (solid and dotted), which are nearly indistinguishable.

4.3. Performance of high-pressure diamond windows

In our experience, we found that the parasitic scattering from diamond windows depends strongly upon the particular diamond and the location through which the beam travels. Three diamonds selected as high-pressure windows were each mounted in a window holder and compared. Diamond 1 (Figs. 6*a* and 6*c*) showed very little scattering around the beamstop, while diamond 2 (Fig. 6*b* and 6*c*) exhibited intense and azimuthally asymmetric scattering. The integrated SAXS profiles of all three diamonds at ambient pressure are compared to the system scattering in Fig. 6(*c*).

The intensity of the diamond scattering was also pressure-dependent, and the magnitude of the changes were found to vary depending upon the diamond. Two of the diamonds, diamond 1 which showed the least scattering and diamond 2 which scattered the most, showed little variation with pressure. In comparison, diamond 3 with intermediate scattering intensity showed significant changes in low-q scattering below 100 MPa, making reliable background subtractions difficult. All high-pressure SAXS measurements on proteins were therefore performed with the first pair. Since diamond 2 had asymmetric scattering, this window would be fixed during the course of the experiment to yield reproducible background scattering. Sample cells were loaded by removing the window containing diamond 1. The high-q region of the diamond SAXS profiles was comparatively featureless, but the intensity decreased with pressure, reflecting the reduction in transmission due to the increased water density and deflection of the windows. Because the high-q region can contain information about the shape of proteins, protein and buffer measurements were taken at the same pressure before subtraction.

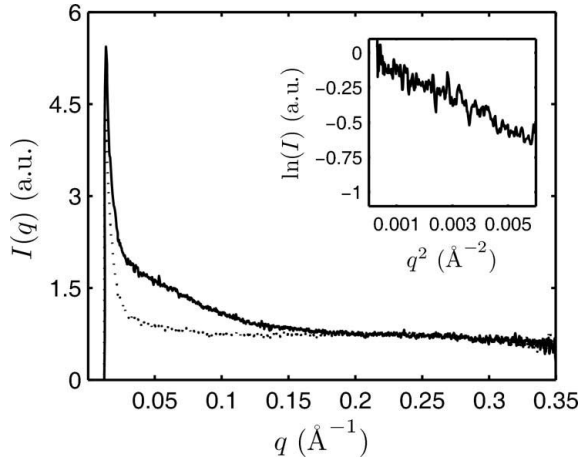

Figure 5
Transmission-normalized scattering profiles of 4 mg ml^{-1} L99A T4 lysozyme, 50 m*M* glycine 100 m*M* NaCl pH 3.0 (solid), and the corresponding buffer (dotted) measured in an acrylic sample cell separately from the high-pressure cell. The inset shows a Guinier plot of subtracted scattering intensity. The radius of gyration is 16.5 (3) Å.

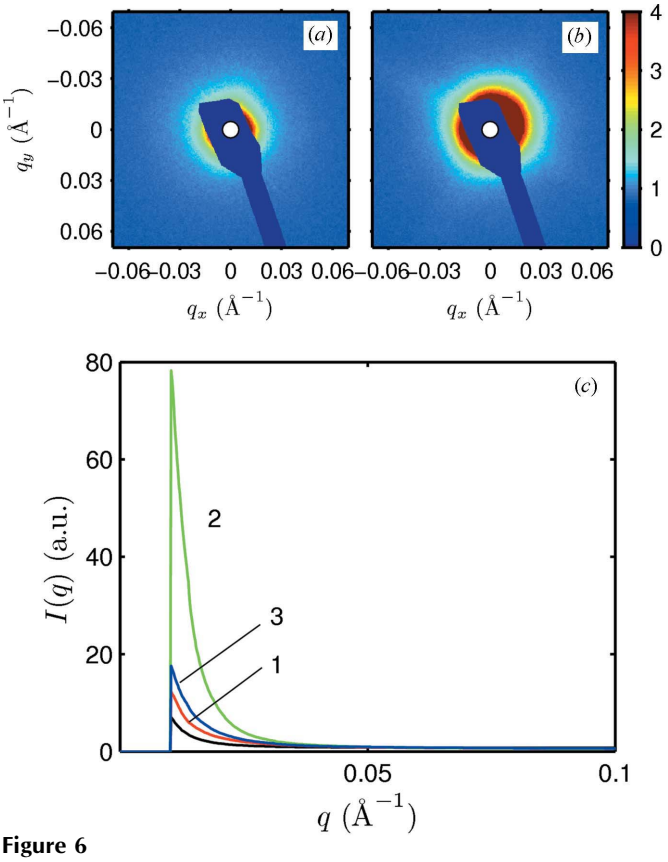

Figure 6
Comparison of the parasitic scattering from three natural diamond windows. (*a*) The SAXS image of diamond 1 shows little scattering around the beamstop, which is shown in dark blue with the beam center marked with a (white) circle. (*a*) The SAXS image of diamond 2 shows intense azimuthally asymmetric scattering near the beamstop. (*c*) Transmission-normalized one-dimensional scattering profiles of the system (black, bottom curve), diamond 1 (red curve), diamond 2 (green curve) and diamond 3 (blue curve).

4.4. Performance of high-pressure SAXS cell

The performance of the high-pressure SAXS cell is demonstrated by the low-pressure and high-pressure data taken on L99A T4 lysozyme. NaCl and protein concentrations were adjusted to minimize inter-protein interactions. Reproducible alignment of the high-pressure cell with respect to the X-ray beam allowed background subtraction to a minimum q value of around 0.024 Å^{-1} at all pressures. The Guinier region was unambiguous for the largely folded and unfolded states of L99A T4 lysozyme.

At 28 MPa, L99A T4 lysozyme was still mostly folded (Fig. 7). The radius of gyration obtained by a Guinier fit over q = 0.024–0.076 Å^{-1} was 17.1 (1) Å, approximately that measured at ambient pressure (see §4.2). At higher pressure, several factors conspire to make accurate measurements of the radius of gyration more difficult. As a protein unfolds, it expands, and the scattering profile shifts to lower q where the parasitic scattering is worse, making background subtraction more challenging. In cases such as these, it becomes even more critical that the background scattering remain reproducible. Guinier analysis was relatively straightforward for L99A T4 lysozyme at high pressure because of the relative compactness

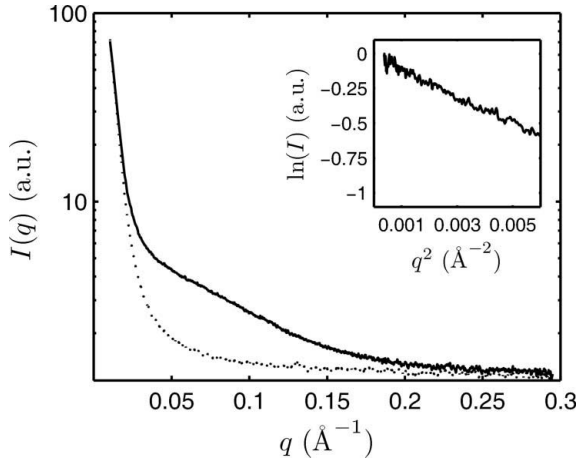

Figure 7
Transmission-normalized scattering profiles of 10 mg ml^{-1} L99A T4 lysozyme, 50 m*M* glycine 100 m*M* NaCl pH 3.0 (solid), and the corresponding buffer (dotted) measured in the high-pressure SAXS cell at 28 MPa. The inset shows a Guinier plot of subtracted scattering intensity. The radius of gyration is 17.1 (1) Å.

of the unfolded state at pH 3.0. The radius of gyration of the unfolded state obtained by a Guinier fit over q = 0.024–0.038 Å^{-1} was 31.6 (17) Å (Fig. 8). A second reason for the increased difficulty of background subtraction at high pressure is specific to high pressure and is caused by the decreasing protein–solvent electron density contrast. As the compressibility of water is roughly one order of magnitude greater than that of proteins, the electron density contrast decreases with increasing pressure. This can be demonstrated with WT T4 lysozyme, which did not unfold below 400 MPa at pH 3.0. The radius of gyration of WT T4 lysozyme did not change appreciably, as can be seen by the unchanging shape of the SAXS profiles with pressure, but the scattering intensity at zero q decreased with pressure (Fig. 9). The zero-angle scattering intensity is a function of the electron density difference between the protein and the solvent. Confidence in the results

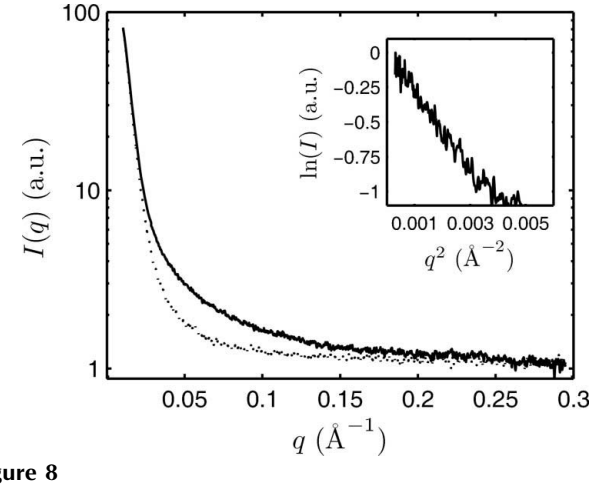

Figure 8
Transmission-normalized scattering profiles of 10 mg ml^{-1} L99A T4 lysozyme, 50 m*M* glycine 100 m*M* NaCl pH 3.0 (solid), and the corresponding buffer (dotted) measured in the high-pressure SAXS cell at 300 MPa. The inset shows a Guinier plot of subtracted scattering intensity. The radius of gyration is 31.6 (17) Å.

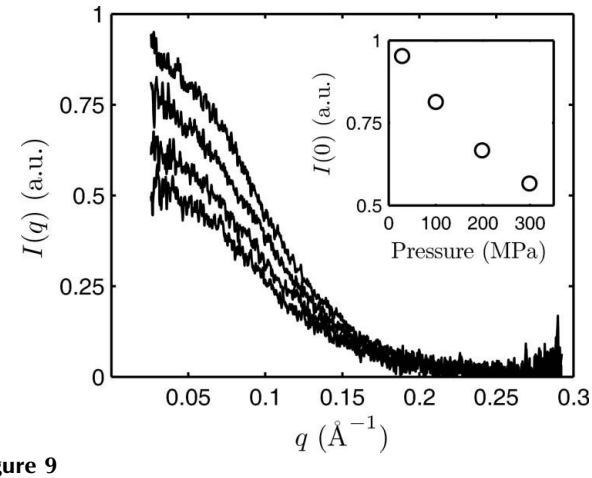

Figure 9
Buffer-subtracted scattering profiles of 16 mg ml^{-1} WT T4 lysozyme in 50 m*M* glycine 150 m*M* NaCl pH 3.0 at 28, 100, 200 and 300 MPa (top to bottom). The radius of gyration does not depend on pressure, as indicated by the unchanging shape of the scattering profiles. The inset shows the corresponding decrease in zero-angle scattering intensity with pressure due to the reduction in protein–solvent electron density contrast.

was obtained by thoroughly checking the reproducibility of the parasitic scattering and repeating the protein SAXS measurements.

5. Conclusions

SAXS is a powerful method to measure structural information of proteins. Owing to the weak scattering signal of proteins, these measurements are typically difficult and place stringent requirements on SAXS cells. With our high-pressure SAXS cell, we have demonstrated successful collection of SAXS from a protein solution under high pressure. The Guinier analysis of T4 lysozyme under pressure shows that we can reproduce the parasitic scattering in the low-q region that is often crucial for interpretation of SAXS data. This permits us to produce accurate protein scattering profiles over a wide q range, opening exciting opportunities for high-pressure studies of proteins. A variety of analyses may be performed on such scattering profiles. The radius of gyration and zero-angle scattering intensity of unfolding and subunit dissociation processes can be extracted from Guinier analysis. Additional structural information of monodisperse samples can be produced from pair distance distribution analysis and molecular envelope reconstruction (Svergun & Koch, 2003).

Because of the limited time available during synchrotron experiments and the complexity of high-pressure experiments, we required an apparatus that is reliable and easy to use at biologically relevant experimental conditions. The use of disposable internal sample cells greatly facilitated this. We found that only one or two persons are necessary during a typical synchrotron experiment. While the internal sample cells were designed for protein solution samples, they would also be suitable for a variety of other samples. Where necessary, the material choices can be modified for compatibility (Wedekind *et al.*, 2006). For very large macromolecules, the scattering at lower q must be recorded. The primary limitation of the current cell is the low-angle scattering from the diamond windows. Different sources of diamond windows are being investigated for a possible reduction in the scattering at low q. Note that because the diamonds are transparent to a wide spectrum of light, this apparatus can be used with probes other than X-rays with small modifications or additions. We have coupled a UV light source to our high-pressure cell for fluorescence measurements and used the cell to observe pressurized samples under the microscope.

To extend the maximum operating pressure above 400 MPa, the design must be re-optimized. The elastic limit of the body of the high-pressure cell is a function of the yield strength of the material and the dimensions [equation (1)]. Because Inconel 725 in the age-hardened state features tensile properties that are difficult to surpass, the dimensions must be changed to increase the elastic limit. Although the elastic limit is not the absolute pressure limit of our cell, we do not exceed this pressure in order to extend its lifetime. The windows will also require modifications to withstand higher pressure. The diamond thickness must be increased or the aperture size must be reduced. Such changes, however, affect other properties, such as the resolution limit of the high-pressure cell.

Finally, as with other X-ray techniques, radiation damage is ultimately the limiting factor in solution SAXS studies of biological materials. The extent of radiation damage depends upon the sample and the experimental conditions. We have seen that radiation-damage-induced aggregation of a highly charged protein depended upon the presence of counterions. We have also observed that multiple short exposures can be less damaging than one long exposure and that pauses between exposures can in some cases recover the undamaged scattering profile. We believe that these are related to the diffusion rate of the aggregates. Radiation damage can be suppressed to a certain extent by the choice of X-ray energy. By tuning beam transmission through the samples, we can optimize the balance between radiation damage and the scattering signal from the proteins. With our samples, we are generally limited to total exposure times of the order of 10–100 s at 10^{12} photons per second before radiation damage irreversibly distorts the scattering profile. In a high-pressure study where one wishes to take measurements from the same sample at multiple pressures, the exposure limit poses a problem. Samples must be changed fairly frequently. A next-generation high-pressure SAXS cell may incorporate a flow cell mechanism to overcome this problem.

The authors thank Professor Roland Winter (University of Dortmund) for discussion of his high-pressure design and Dr Testuro Fujisawa (RIKEN Harima Institute/SPring-8) for his insight. Our high-pressure SAXS cell would not have been possible without the help of Professor William A. Bassett (Cornell University), who provided and polished the diamond windows, and the guidance of Dr Chang-Sheng Zha (Carnegie Institute of Washington). We would like to give special thanks to the group of Professor Brian W. Matthews (University of

Oregon) for providing T4 lysozyme and Special Metals Corporation (Huntington, WV) for providing annealed Inconel 725 and age-hardening service. For their help with data acquisition, the authors are grateful to Buz Barstow, Gil Toombes, Lucas Koerner, Marcus Collins, Chae Un Kim, Fred Heberle and Darren Southworth, as well as CHESS staff members Arthur Woll, Peter Busch and Richard Gillilan. We acknowledge support from the Cornell Center for Materials Research (an NSF MRSEC), the NIH *via* a Protein Structure Initiative grant to the Hauptmann–Woodward Institute, the office of Biological Environmental Research of the DOE, and CHESS, an NSF-DMR/NIH-NIGMS-supported National Facility under NSF award DMR-0225180.

References

Akasaka, K. & Yamada, H. (2001). *Methods Enzymol.* **338**, 134–158.
Blanton, T., Huang, T., Toraya, H., Hubbard, C., Robie, S., Louer, D., Gobel, H., Will, G., Gilles, R. & Raftery, T. (1995). *Powder Diffr.* **10**, 91–95.
Bridgman, P. W. (1914). *J. Biol. Chem.* **19**, 511–512.
Brun, L., Isom, D. G., Velu, P., García-Moreno, B. & Royer, C. A. (2006). *Biochemistry*, **45**, 3473–3480.
Collins, M. D., Hummer, G., Quillin, M. L., Matthews, B. W. & Gruner, S. M. (2005). *Proc. Natl Acad. Sci. USA*, **102**, 16668–16671.
Dzwolak, W., Kato, M. & Taniguchi, Y. (2002). *Biochim. Biophys. Acta*, **1595**, 131–144.
Erbes, J., Winter, R. & Rapp, G. (1996). *Ber. Bensenges. Phys. Chem.* **100**, 1713–1722.
Eremets, M. (1996). *High Pressure Experimental Methods.* Oxford University Press.
Ferrão-Gonzales, A. D., Souto, S. O., Silva, J. L. & Foguel, D. (2000). *Proc. Natl Acad. Sci. USA*, **97**, 6445–6450.
Field, J. E. (1979). *The Properties of Diamond.* London: Academic Press.
Frye, K. J. & Royer, C. A. (1998). *Protein Sci.* **7**, 2217–2222.
Fujisawa, T., Kato, M. & Inoko, Y. (1999). *Biochemistry*, **38**, 6411–6418.
Gross, M. & Jaenicke, R. (1994). *Eur. J. Biochem.* **221**, 617–630.
Harano, Y. & Kinoshita, M. (2006). *J. Chem. Phys.* **125**, 24910.
Heremans, K. & Smeller, L. (1998). *Biochim. Biophys. Acta*, **1386**, 353–370.
Holzapfel, W. B. & Isaacs, N. S. (1997). Editors. *High-Pressure Techniques in Chemistry and Physics: A Practical Approach*. Oxford University Press.
Huang, T. C., Toraya, H., Blanton, T. N. & Wu, Y. (1993). *J. Appl. Cryst.* **26**, 180–184.
Hummer, G., Garde, S., García, A. E., Paulaitis, M. E. & Pratt, L. R. (1998). *Proc. Natl Acad. Sci. USA*, **95**, 1552–1555.
Imai, T., Ohyama, S., Kovalenko, A. & Hirata, F. (2007). *Protein Sci.* **16**, 1927–1933.
Jonas, J. (2002). *Biochim. Biophys. Acta*, **1595**, 145–159.
Meersman, F., Smeller, L. & Heremans, K. (2002). *Biophys. J.* **82**, 2635–2644.
Mozhaev, V. V., Heremans, K., Frank, J., Masson, P. & Balny, C. (1996). *Proteins*, **24**, 81–91.
Nishikawa, Y., Fujisawa, T., Inoko, Y. & Moritoki, M. (2001). *Nucl. Instrum. Methods Phys. Res. Sect. A*, **467–468**, 1384–1387.
Northrop, D. B. (2002). *Biochim. Biophys. Acta*, **1595**, 71–79.
Paladini, A. A. & Weber, G. (1981). *Biochemistry*, **20**, 2587–2593.
Paliwal, A., Asthagiri, D., Bossev, D. P. & Paulaitis, M. E. (2004). *Biophys. J.* **87**, 3479–3492.
Panick, G., Malessa, R., Winter, R., Rapp, G., Frye, K. J. & Royer, C. A. (1998). *J. Mol. Biol.* **275**, 389–402.
Panick, G., Vidugiris, G. J., Malessa, R., Rapp, G., Winter, R. & Royer, C. A. (1999). *Biochemistry*, **38**, 4157–4164.
Pin, S., Royer, C. A., Gratton, E., Alpert, B. & Weber, G. (1990). *Biochemistry*, **29**, 9194–9202.
Poulter, T. C. (1932). *Phys. Rev.* **40**, 861–871.
Pressl, K., Kriechbaum, M., Steinhart, M. & Laggner, P. (1996). *Rev. Sci. Instrum.* **68**, 4588–4592.
Royer, C. A. (2002). *Biochim. Biophys. Acta*, **1595**, 201–209.
Ruan, K.-C. & Balny, C. (2002). *Biochim. Biophys. Acta*, **1595**, 94–102.
Silva, J. L., Foguel, D., Poian, A. T. D. & Prevelige, P. E. (1996). *Curr. Opin. Struct. Biol.* **6**, 166–175.
Silva, J. L. & Weber, G. (1993). *Annu. Rev. Phys. Chem.* **44**, 89–113.
Spain, I. L. & Paauwe, J. (1977). *High Pressure Technology.* New York: Marcel Dekker.
Svergun, D. I. & Koch, M. H. J. (2003). *Rep. Progr. Phys.* **66**, 1735–1782.
Torrent, J., Alvarez-Martinez, M. T., Liautard, J.-P. & Lange, R. (2005). *Biochim. Biophys. Acta*, **1764**, 546–551.
Wedekind, J. E., Gillilan, R., Janda, A., Krucinska, J., Salter, J. D., Bennett, R. P., Raina, J. & Smith, H. C. (2006). *J. Biol. Chem.* **281**, 38122–38126.
Winter, R. (2002). *Biochim. Biophys. Acta*, **1595**, 160–184.
Woenckhaus, J., Kohling, R., Winter, R., Thiyagarajan, P. & Finet, S. (2000). *Rev. Sci. Instrum.* **71**, 3895–3899.
Zipp, A. & Kauzmann, W. (1973). *Biochemistry*, **12**, 4217–4228.